



Heavy metal adsorptive application of hydrolyzed corn starch

Chukwunonso O. Aniagor¹ · M. A. Afifi² · A. Hashem²

Received: 30 June 2021 / Accepted: 23 September 2021 / Published online: 5 October 2021
© The Polymer Society, Taipei 2021

Abstract

Starch is an abundant natural and renewable carbohydrate polymer, with cation sorption deficiency due to its high crystallinity and amylose content which causes substantive mass transfer resistance during adsorption. Therefore, the present study synthesized polyacrylonitrile grafted starch (graft-starch) that was subjected to heat treatment and saponification reaction to facilitate a partial transformation of the available amide groups (due to copolymer grafting) into carboxylate groups. The reactions afforded the desired polyacrylonitrile-grafted starch hydrogel ('*Poly-g-Hyd*') which was further utilized for zinc ion uptake. It was observed that the polar nitrile (CN) groups of the grafted polyacrylonitrile substantially improved the '*Poly-g-Hyd*' water absorption capacity and cation binding interaction, as well as entrenched stable network chains that are insoluble in water. The water absorption and zinc ion sorption capacities of 490 g water/g '*Poly-g-Hyd*' and 508.85 mg/g, were respectively recorded. Furthermore, the optimum adsorption conditions were established at pH 5.0, 20 min and 0.3 g/L, while the Freundlich and pseudo-second-order models provided the best fit to the isotherm and kinetic data, respectively. The study, therefore, demonstrated the effectiveness of '*Poly-g-Hyd*' in the uptake of aqueous zinc ions.

Keywords Starch hydrogel · adsorption · zinc ion · isotherm · kinetics

Introduction

The rapid industrialization and world population growth have caused a surge in ecosystem toxicity due to the presence of aqueous heavy metal contamination [1–3]. The ecotoxicological dangers associated with these heavy metal ion accumulations in the aquatic environment is primarily linked to their poor degradability [4]. Our choice adsorbate, zinc ions (Zn^{2+}) has extensive application in process industries (in steelwork, galvanization, brass plating, fibre manufacturing, dye & pigment, etc.) [5]. When the contaminated waste streams from these industries are poorly treated before discharge into the environment, zinc ions could find their way into the food chain of living species [6]. Although zinc is an essential element, its high-level accumulation in living

species could cause grave health damage [7, 8]. Some of its adverse health impacts include depression, inactivity, abnormal neurological functionality, etc. [9]. The World Health Organization (WHO) stipulated a 5.0 mg L^{-1} limit for aqueous zinc ion contamination [10], however, literature reports showed a zinc ion concentration in the range of $1 \geq Zn^{2+} \geq 48000 \text{ mgL}^{-1}$ from different waste streams [4].

Considering the aforementioned health impacts of heavy metal ion pollution, worthwhile research into the various approaches for the reduction of their (heavy metal ions) concentration in waste streams to within the WHO permissible limits is plausible. Various approaches, such as coag-flocculation, membrane filtration, ion exchange, etc. have been previously adopted for aqueous zinc ion treatment, with several associated drawbacks (like high cost, poor treatment efficiency, etc.) [8]. Meanwhile, biosorption has been regarded as a promising treatment option due to its treatment efficiency, cost-effectiveness, operational flexibility, etc. [11–13].

Many adsorbents, including natural carbohydrate polymers (starch), have been extensively reported as efficient for aqueous heavy metal ion biosorption. These materials were either used raw [14–16] or with some form of chemical modifications [17, 18]. Meanwhile, the cation sorption

✉ Chukwunonso O. Aniagor
co.aniagor@unizik.edu.ng

✉ A. Hashem
alishashem2000@yahoo.com

¹ Department of Chemical Engineering, Nnamdi Azikiwe University, P.M.B. 5025, Awka, Nigeria

² Textile Research Division, National Research Centre, Dokki, Cairo, Egypt

capacity of these raw starch is limited by their high crystallinity and amylose content [19]. They also hamper the diffusion of the cations into the polymer chelation sites [5]. To forestall such limitation, researchers have attempted the chemical modification/functionalization (via improvement of the available functional groups) of these native carbohydrate polymers, aimed at yielding efficient adsorbents, with superior heavy metal sorption capacity [8]. This is because their (carbohydrate polymers) cation sorption efficiency is a function of the electrostatic complexation, governed by the adsorbate-adsorbent surface charge differences [20]. Polymer sorbent functionalization could be achieved through different chemical techniques like copolymer grafting, hydrolysis, etc. [21]. Copolymer grafting (using suitable monomer), an important functionalization avenue could successfully introduce important metal-binding sites such as carboxyl, amino group, etc., as well as significantly modify the starch/polymer network [5, 22].

Therefore, the present study involved the synthesis of polyacrylonitrile grafted starch (graft-starch) which was subjected to heat treatment and subsequent saponification reaction to facilitate a partial transformation of the entrenched amide groups into carboxylic groups. The reactions afforded the desired polyacrylonitrile-grafted starch hydrogel ('*Poly-g-Hyd*') which was then utilized for zinc ion uptake. The objectives of the study are stated thus; (a) to measure the nitrogen content of the synthesized hydrogel, as well as their swelling capacity (b) to characterize the synthesized '*Poly-g-Hyd*' using FTIR, SEM, and SEM-EDX, (c) to evaluate the effect of contact time, adsorbent dosage and adsorbate solution pH on the adsorption capacity (c) to elucidate the isotherm, kinetics and mechanism of the adsorption process.

Materials and methods

Materials

The starch precursor (maize starch) used in the study was obtained from the Egyptian Starch and Glucose Manufacturing Company, Cairo, Egypt. The acrylonitrile, ammonium cerium (IV) nitrate (CAN), zinc acetate, caustic soda, hydrogen trioxonitrate (v) acid, ethanoic acid, acetone, methanol, ethyl alcohol and all other employed reagents were all laboratory grade chemicals, supplied by Merck, Germany.

Methods

Synthesis of the grafted starch

The copolymerized (graft) starch was synthesized following the procedure earlier reported by Abdel-Halim [23], with slight modifications. The procedure involved the gelatination

of a specific amount of maize starch in suitable (enough to form a gel) volume of water followed by heat treatment of the resultant starch gel (at 85 °C for 30 min) and subsequent addition (30 ± °C and stirring at 150 rpm) of a specific volume of acrylonitrile, together with a binary mixture of freshly prepared ammonium cerium (iv) nitrate and 1 N HNO₃ to afford the starch copolymer. The reaction by-products (homopolymers) were further eliminated via the precipitation of the starch copolymer in N, N-dimethylformamide (DMF). The resultant precipitates (homopolymer-free graft-starch) was obtained, washed with deionized water and then oven-dried at 50 °C to constant dry weight.

Following the micro-Kjeldahl method [24], the % nitrogen content of the graft-starch was estimated, while the % graft yield was evaluated from Eq. (1) [17, 25].

$$\% \text{Graftyield} = \frac{\left[\frac{(N(\%)*53)}{14} * 100 \right]}{\left[\frac{100 - (N(\%)*53)}{14} \right]} \quad (1)$$

NB 53 and 14 is the molar mass of acrylonitrile and Nitrogen (g/mol), respectively.

Hydrogel synthesis

10 mL of 0.7 N sodium hydroxide solution was added to 1.0 g of the graft-starch contained in a loosely stoppered (to permit ammonia evolution) flask, followed by mechanical stirring at 150 rpm and 95 °C. A subsequent change in the colour of the solution (from deep red to light yellow informs the climax of the saponification reaction. Furthermore, the saponified starch was contacted with a predetermined volume of methanol, stirred for 5 min and excess volume of ethanol was subsequently added to the mixture. The precipitate so obtained was washed with acidified ethanol (until neutral pH), filtered off, oven-dried (60 °C, 3 h) to afford the superabsorbent hydrogels ('*Poly-g-Hyd*').

Hydrogel swelling capacity measurement

The measurement was achieved via the impregnation of a predetermined amount of the synthesized '*Poly-g-Hyd*' in a suitable volume of distilled water (at 30 ± 3 °C) until its saturation. The fully swollen '*Poly-g-Hyd*' was recovered as filtrate, drained and reweighed. Its water absorption capacity was then evaluated from Eq. (2) [23, 25].

$$\text{Swelling capacity} \left(\frac{\text{g}}{\text{g}} \right) = \frac{M_2 - M_1}{M_1} \quad (2)$$

Where M₁ and M₂ are the Masses of swollen '*Poly-g-Hyd*' and dry '*Poly-g-Hyd*'.

Hydrogel characterization

The surface chemistry/functional groups on the raw and spent hydrogel, as well as that of the hydrogel precursor, was elucidated via FTIR (Perkin–Elmer Spectrum1000 spectrophotometer) at 4000–400 cm^{-1} and scan-interval of 1 cm^{-1} (over 120 scans). Similarly, the surface morphology was obtained via SEM measurement [TESCAN CE VEGA 3 SBU (117-0195- Czech Republic)] at 1000x magnification. Before the SEM analysis, the samples were mounted on a standard microscope stub and coated with a thin gold layer. Consequently, the presence of the adsorbed zinc ions on the adsorbent was informed from the Energy-dispersive X-ray (EDX) patterns.

Adsorption experiments

By dissolving an appropriate amount of zinc acetate in deionized water, the zinc ion stock solution (1 g L^{-1}) was obtained. Meanwhile, the working zinc ion concentrations were further achieved from the serial dilution (using deionized water) of the stock solution.

During the adsorption experiment, a predetermined amount of ‘Poly-g-Hyd’ was charged into the adsorbate solution (100 mL) contained in a 250 mL conical flask. The mixture was stirred mechanically on a magnetic stirrer (Stuart, Model UC151/120V/60) at 150 rpm and 30 °C. At a specified interval, test samples were withdrawn from the mixture, filtered through Whatman No. 41 filter paper and the remaining Zn (II) ion concentration was measured using atomic absorption spectrophotometer (AAS, ZA3000, HITACHI, Japan). By varying the solution pH using either 0.1 M HNO_3 or 0.1 M NaOH as appropriate, the effect of pH studies was investigated in the pH range of 2.0–7.0. Similarly, the effect of time (0–60 min) and adsorbent dosage (0.3–4.0 g/L) was also investigated.

The associated adsorption parameters such as the % uptake efficiency (RE %), as well as the amount of zinc ion adsorbed at equilibrium (q_e) are calculated from Eqs. (3) and (4), respectively.

$$\text{RE (\%)} = \frac{C_o - C_e}{C_o} \cdot 100\% \quad (3)$$

$$q_e = \frac{(C_o - C_e)V}{W} \quad (4)$$

Where C_o = Initial zinc ion concentration (mg L^{-1}), C_e = zinc ion concentration at equilibrium (mg L^{-1}), W = Mass of ‘Poly-g-Hyd’ used (g), V = volume of adsorbate solution used (L).

Results and discussion

Adsorbent characterization result

Physicochemical analyses

The % nitrogen content on the synthesized hydrogel (‘Poly-g-Hyd’) as shown in Table 1 provide information on the extent of the copolymer grafting. The result shows a depletion in the % nitrogen content of the grafted starch following the saponification reaction towards the hydrogel synthesis. This finding could be linked to the transformation of some of the cyano groups on the grafted starch to amide ($-\text{CONH}_2$) and carboxylate ($-\text{COONa}$) groups, although the carboxylate groups were subsequently at the later stage of the hydrogel synthesis process.

According to the value depicted in Table 1, ‘Poly-g-Hyd’ showed a relatively high absorption capacity of 490 g water/g ‘Poly-g-Hyd’, which could be due to the structural changes occurring during the sequence of steps involved in the copolymer grafting. For instance, it is believed that the gelatination effect could be responsible for significant physicochemical changes (such as molecule disorientation, free volume magnification, etc.) observed on the starch structure [17]. Similarly, the polymer crosslinking due to the copolymer grafting significantly improved the ‘Poly-g-Hyd’ structural network [23].

Scanning Electron micrograph

The morphology of the maize starch (precursors), ‘Poly-g-Hyd’ and Zn (II)-loaded ‘Poly-g-Hyd’ was obtained using SEM imagery and presented in Fig. 1. As shown in Fig. 1a, the raw starch resembled a woollen matrix, with fibrous interconnections and substantial surface heterogeneity. Meanwhile, the hydrolysed grafted starch (Fig. 1b) showed better surface aggregated patches, with evidence of particle agglomeration into more pronounced irregular shapes of superior surface roughness and porosity. Furthermore, the previously intact starch polymeric networks observed in Fig. 1a partially crumbled into loosely bound biofilm-like amorphous matrices (Fig. 1b) sequel to hydrogel formation. This improved surface roughness and porosity is a direct consequence of the precipitation stage, which eliminated the

Table 1 Characteristics of ‘Poly-g-Hyd’

N % in poly (AN)-starch graft copolymer	N % in ‘Poly-g-Hyd’	Swelling capacity (g/g)
11.40	3.10	490.0

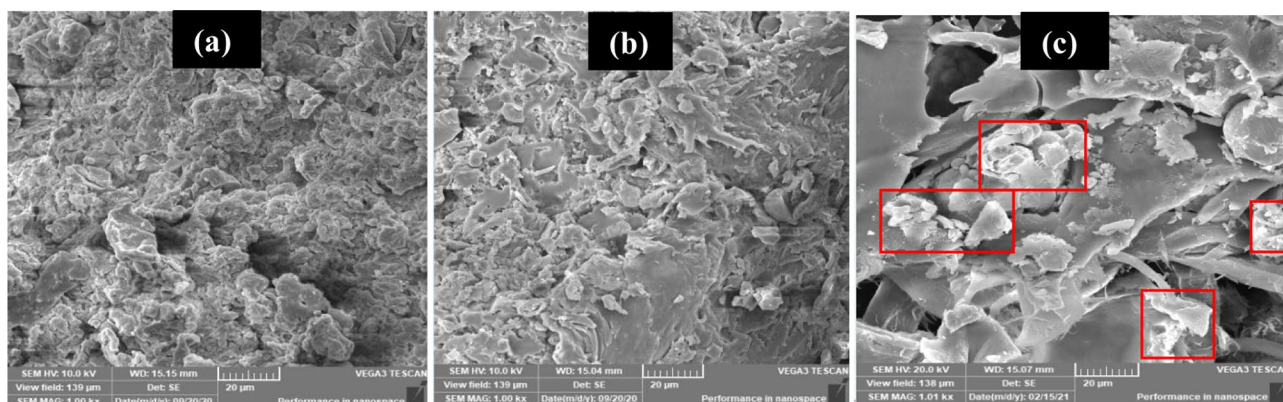


Fig. 1 SEM images for (a) maize starch (b) 'Poly-g-Hyd' and (c) Zn (II)-loaded 'Poly-g-Hyd'

solubilized low molecular weight homopolymer. Furthermore, the flake-like smoothed surface morphology, with no surface roughness and porosity observed in Fig. 1c, is an indication of the presence of the adsorbed heavy metal cation on the adsorbent pores.

Energy dispersion X-ray (EDX) study

Elemental mapping and % mass distribution on the spent adsorbent (Zn (II)-loaded 'Poly-g-Hyd') is inscribed into Fig. 2. The considerable presence of carbon (13.50%) and oxygen (21.45%), which are the main component of starch compounds was observed in the EDX mapping spectrum, as well as the presence of the adsorbed zinc (11.59%) ion. The observed presence of zinc ions in the post adsorption EDX spectrum confirms their adhesion onto the adsorbent. Furthermore, the nitrogen group that was introduced onto the starch material during its copolymerization with the acrylonitrile was not identified in Fig. 2. This development confirmed the exhaustion of these nitrogen groups as a result of cation chelation.

Surface chemistry

Figure 3 shows the FTIR spectra for raw starch, grafted starch, 'Poly-g-Hyd' and Zn (II)-loaded 'Poly-g-Hyd'. The H-bonded OH stretch (assigned to bands existing around 3400 cm^{-1}), C - H stretch (around 2900 cm^{-1}), amide/carboxylate C=O stretch ($1720\text{--}1550\text{ cm}^{-1}$), C - C stretch ($1400\text{--}1200\text{ cm}^{-1}$) and C - O stretch (around 1150 cm^{-1}) are the major functional groups common in all the spectra (Fig. 3). Upon the comparison of the different spectra, it was observed that the C - H stretch of the raw starch was suppressed sequel to copolymer grafting operation. Similarly, the C \equiv N and C \equiv C groups, respectively identified on the grafted starch and raw starch spectra consequently disappeared in the 'Poly-g-Hyd' (Fig. 3). Furthermore, the diminished C=O stretch peak on the grafted and raw starch became more pronounced on the 'Poly-g-Hyd' spectra. A conspicuous nitrile (C \equiv N) group identified at 2237 cm^{-1} on the grafted starch spectra affirmed the success of the copolymer grafting. The FTIR spectra of the post adsorption

Fig. 2 Energy dispersion x-ray mapping spectrum

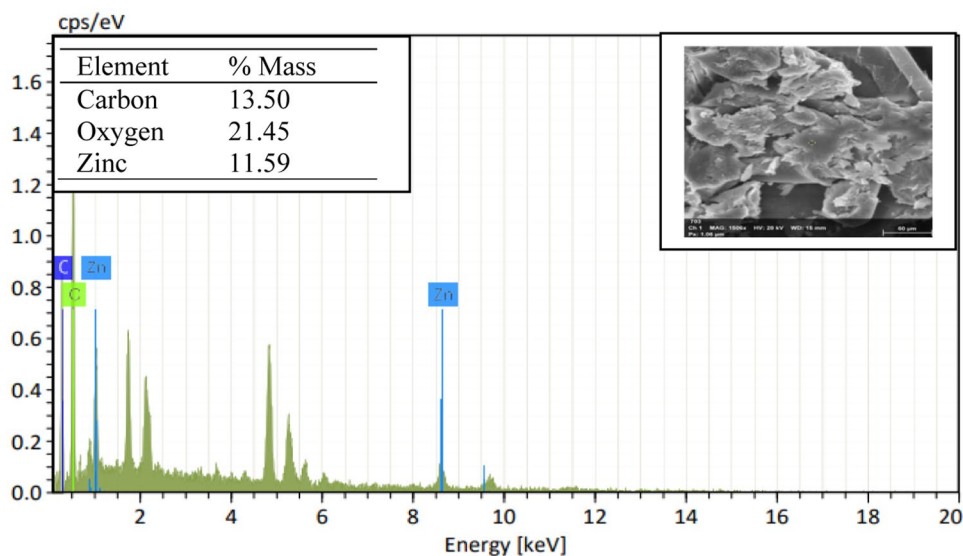
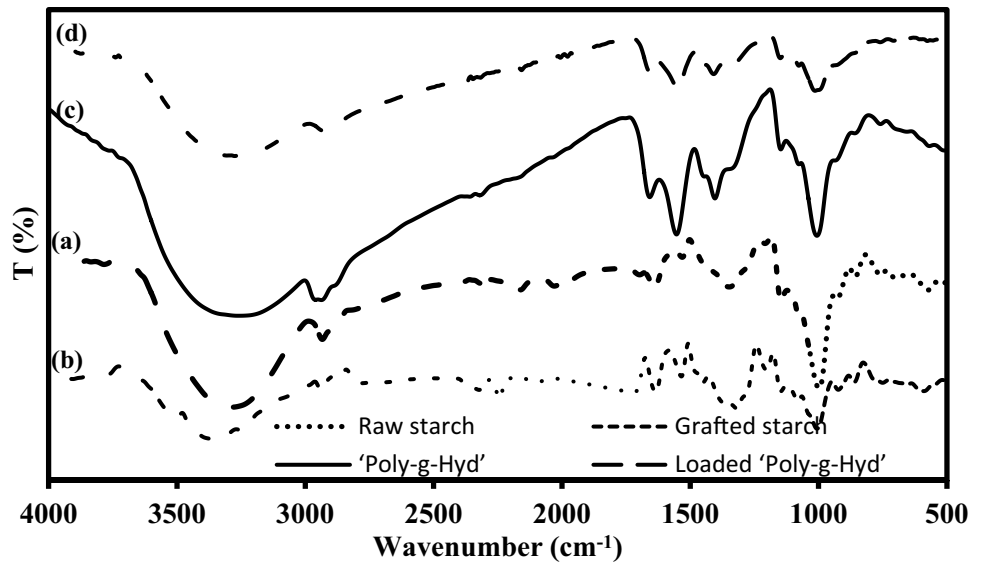


Fig. 3 FTIR spectra for (a) raw starch (b) grafted starch (c) 'Poly-g-Hyd' (d) Loaded 'Poly-g-Hyd'



sample did not differ much from that of the unused adsorbent, except for the observed reduction in peak intensity.

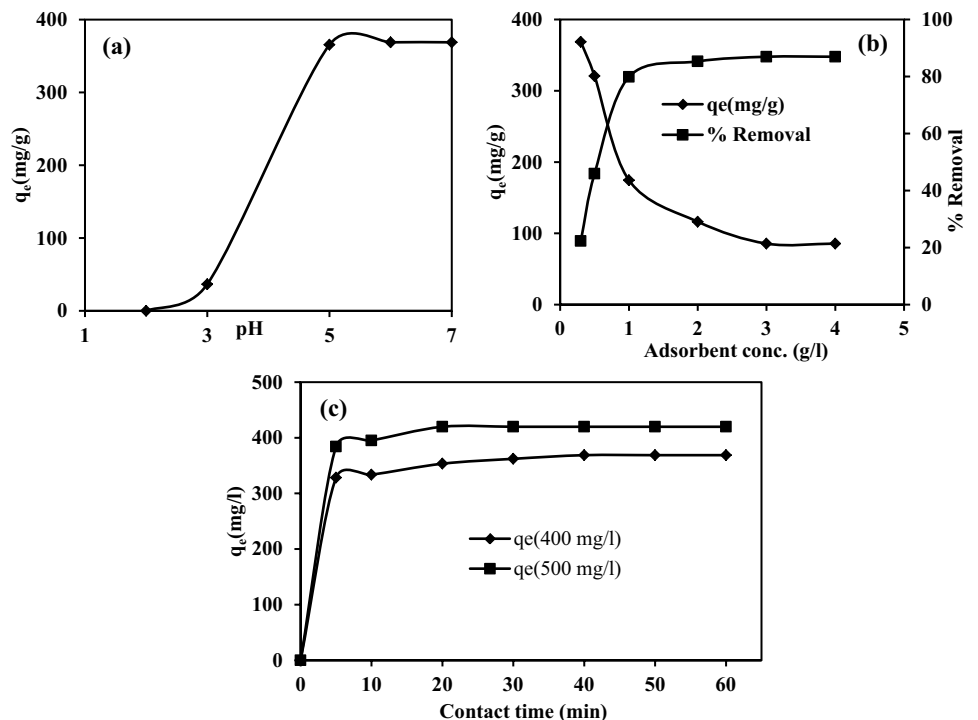
Effect of the process variables

Effect of solution pH

The pH of the adsorbate solution and the surface charge of the adsorbent (point of zero charge) is crucial for determining the extent of the adsorbate-adsorbent complexation

and interaction [26]. Considering the pH_{pzc} of 'Poly-g-Hyd', which was recorded at pH 2.4 (plot not shown), the operational pH for the study was obtained at pH above pH 2.4 (Fig. 4a). This observation is so much as expected because, at a lower pH ($pH < pH_{pzc}$), the adsorption sites on the 'Poly-g-Hyd' were mostly protonated, such that the hydrogen ion (H^+) tends to compete with cations. A steady increment in the solution pH towards and above the pH_{pzc} expectedly resulted in substantive negativity of the adsorbents' surface charge, thus allowing for increased cation affinity and subsequent binding [27]. For instance, no

Fig. 4 The plot of the effect of (a) solution pH on the adsorbed amount (b) adsorbent dose on the % removal and adsorbed amount (c) variation of contact time and initial concentration on the adsorbed amount



observable zinc cation uptake occurred at pH 2.0, hence the adsorption capacity at that pH was 0. Similarly, only 10% (36.54 mg/g) of the total adsorption capacity recorded at optimum condition was realised at pH 3.0. Meanwhile, at an optimum condition of pH 5.0, the highest adsorption capacity of 365.44 mg/g was recorded.

Effect of adsorbent dosage

The effect of the adsorbent dosage on cation uptake capacity and removal efficiency was simultaneously investigated and the finding is shown in form of a plot in Fig. 4b. It is observed that the removal efficiency varies inversely with the adsorption capacity. Meanwhile, the relationship between that adsorbent dosage and adsorption capacity will be emphasized in this discussion. This is because the adsorption capacity is a function of the intrinsic adequacy of the adsorbent, while the initial adsorbate concentration significantly affects the removal efficiency [28].

Analysis of Fig. 4b showed that an increase in the adsorbent mass (from 0.3 to 1.0 g/L) resulted in a sharp decline (about 47% reduction) in the ‘Poly-g-Hyd’ adsorption capacity. This trend of sustained decrease in the adsorption capacity persisted with an increase in the amount of ‘Poly-g-Hyd’ at every instant. Hence, the adsorption capacity ultimately reduced from 368.761 mg/g (at 0.3 g of ‘Poly-g-Hyd’/litre of adsorbate) to as low as 85.64 mg/g (at 4.0 g of ‘Poly-g-Hyd’/litre of adsorbate). This observation could be linked to the possible active site clogging, overcrowding and their subsequent agglomeration at high adsorbent dosage [26, 29]. Therefore, an optimum ‘Poly-g-Hyd’ mass of 0.3 g/L was subsequently adopted in the study.

Effect of contact time and initial concentration

Adsorption is majorly a mass transfer operation; thus, a sustained extension of adsorption duration is expected to improve the rate of adsorbates’ molecular diffusion from the bulk liquid phase, through the solid-liquid interface and into the adsorbents active sites. The effect of contact time at varying adsorbate initial concentrations was investigated and the finding presented in Fig. 4c. The results showed that about 91% (384.125 mg/g) and 93% (328.153 mg/g) of the optimum adsorption capacities, at the initial concentration of 500 mg/L and 400 mg/L, respectively was realized within the first 5 min of adsorption operation. This observation speaks volumes of the affinity between the ‘Poly-g-Hyd’ and the zinc cation, due to the recorded fast adsorption kinetics [11]. Meanwhile, the remaining 9% and 7% increment in the optimum adsorption capacity for 500 mg/L and 400 mg/L systems, respectively occurred at the brink of adsorption equilibrium at 20 min contact time. This finding suggests a

possible saturation of the ‘Poly-g-Hyd’ active sites [30]. The rapid adsorption rate observed within the first 5 min of operation is related to the availability of a large number of zinc cations (which increased with an increase in adsorbate concentration) and ‘Poly-g-Hyd’ active sites. Conversely, the abated adsorption rate experienced as the process proceeded beyond 5 min until the attainment of equilibrium at 20 min resulted from the active site saturation and reduction in the adsorbate concentration at the bulk liquid phase [31]. Further observation of Fig. 4c shows that the adsorption capacity increased as the initial adsorbate concentration. This phenomenon characterizes a surface reaction, where the concentration induced driving force between the zinc cations and the ‘Poly-g-Hyd’ active sites is strengthened [32, 33].

Equilibrium studies

In this study, the experimental equilibrium data were modelled with four (4) isotherm models namely Langmuir, Freundlich, Temkin, and Dubinin–Radushkevich (D-R) models [34] to obtain the model of best fit. However, the smaller the average percentage error (APE) for a given model as evaluated from Eq. (5), the better the model fit due to reduced error variance between the experimental and model-predicted adsorption capacity values. The import of the respective isotherm model parameters to the present adsorption system is discussed in the subsequent subsections, while the combined isotherm plot and parameter table for all the models are presented in Fig. 5; Table 2, respectively.

$$\text{APE}(\%) = \frac{\sum_{i=1}^n |(q_{e,\text{exp}} - q_{e,\text{pred}})/q_{e,\text{exp}}|}{n} * 100 \quad (5)$$

Where ‘n’ is the number of the experimental data point.

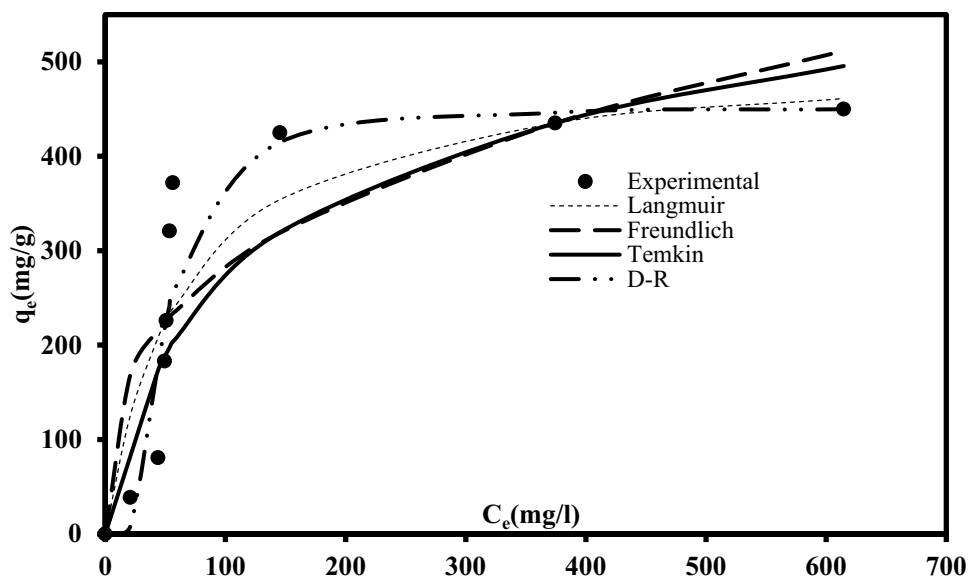
Langmuir model

This model is hinged on the fundamental assumption of monolayer adsorption onto a homogenous adsorbent surface, with identical/energetically uniform adsorption sites. The nonlinear Langmuir model equation and the associated favorability constant (R_L) is expressed as Eqs. (6)–(7) [35]. Where $R_L > 1$, $R_L = 1$, $R_L = 0$ and $0 < R_L < 1$ implies unfavourable, linear, irreversible and favourable nature of the adsorption process, respectively.

$$q_e = \frac{q_m k_L C_e}{1 + k_L C_e} \quad (6)$$

$$R_L = \frac{1}{1 + K_L C_o} \quad (7)$$

Fig. 5 A plot showing the Experimental Langmuir, Freundlich, Temkin and D-R isotherm data



According to Table 2, the model showed a sufficiently large maximum adsorption capacity of 508.859 mg/g. Similarly, the models' separation factor, R_L depicted a positive value of 0.016 ($0 < R_L < 1$), thus suggesting adsorption favorability. Its coefficient of determination (R^2) and APE values of 0.937 and 4.86, respectively is relatively good and within a suitable range but these values are inferior to those recorded by Freundlich and Temkin model. Based on the model of best fit selection criteria, the Langmuir model cannot be regarded as the best fit, however, its predicted data provided a reasonable fit to the experimental data.

Freundlich model

This model is synonymous with heterogeneous multilayer adsorption and uneven adsorption energy distribution [36]. The model is mathematically expressed as Eq. (8), while the model constant (n_F) value suggests the extent of the adsorbent-adsorbate affinity.

$$q_e = K_F (C_e)^{\frac{1}{n_F}} \tag{8}$$

Table 2 Isotherm model parameters

Langmuir	Freundlich	Temkin	D-R*
$q_{max} = 508.859$	$n_F = 3.05$	$A_T = 0.094$	$q_D = 451.99$
$K_L = 8.009$	$K_F = 62.36$	$b_T = 20.63$	$\beta_D = 2.8E-04$
$R_L = 0.016$	$R^2 = 0.987$	$R^2 = 0.917$	$R^2 = 0.966$
$R^2 = 0.937$	APE (%) = 2.80	APE (%) = 3.64	APE (%) = 6.29
APE (%) = 4.86			

The fitting of the equilibrium experimental data to this model (Fig. 5) depicted the highest R^2 and the lowest APE values of 0.987 and 2.80, respectively (Table 2). Based on these values, the model predicted data is believed to have provided the best description of experimental data. Similarly, the evaluated n_F value of 3.05 is well within the expected range ($1 < n_F < 10$), thus implying a favourable interaction between the zinc cation and the 'Poly-g-Hyd' adsorbent. Consequently, the zinc cation sustained a multi-layer binding onto the 'Poly-g-Hyd' surface.

Temkin model

The adsorbate-adsorbent interaction during adsorption is correlated by the Temkin model [37]. The model postulates a uniform distribution of adsorption energy, with a direct variation between the heat of adsorption and surface coverage. Its nonlinear equation is expressed as Eq. (9).

$$q_e = \frac{RT}{b_T} \ln(K_T C_e) \tag{9}$$

The model parameters and their associated goodness of fit (R^2 and APE) values that are presented in Table 2 are reasonable good. For instance, its R^2 value of 0.917 implies that about 90 % of the experimental data was explained by the model predicted data. Similarly, the b_T constant which is related to the adsorption energy variation depicted a positive value. Hence, the increase in temperature of the adsorption system will have a detrimental effect on the entire sorption process. Despite the high R^2 and relatively low APE value, the comparison of the model and experimental isotherm curve (Fig. 5) showed that the Temkin model curve varied widely from the experimental equilibrium curves. Therefore,

although the Temkin isotherm can describe the zinc cation sorption onto 'Poly-g-Hyd', its fitting ability still fell short of those provided by the Freundlich model.

Dubinin–Radushkevich (D-R) model

As an empirical model, Dubinin–Radushkevich isotherm [38], effectively relates the mechanism of heterogeneous surface adsorption, with Gaussian distribution of energy [39, 40]. The model term 'E' which denote the mean free energy and is evaluated from Eq. (10) offers a distinction between physical ($E < 8$ kJ/mol) and chemical adsorption [41]. The D-R model equation is shown in Eq. (11).

$$E = \frac{1}{\sqrt{2\beta_D}} \quad (10)$$

$$q_e = q_D * \exp \left\{ -B_D \left[RT \left(1 + \frac{1}{C_e} \right) \right]^2 \right\} \quad (11)$$

This model showed a reasonably high R^2 value, however, it's the magnitude of its APE value of 6.29 was the largest of all. Figure 5 also showed a wide variation between the experimental isotherm curve and the model curve. This finding portrays the model's inefficiency at describing the experimental equilibrium data. Meanwhile, the magnitudes of the D-R mean energy, E (42.25 KJ/mol), as evaluated from Eq. (10), is larger than 8 kJ/mol; a suggestion for the dominance of chemisorption [42, 43].

Kinetic studies

The experimental kinetic data was modelled using two (2) classical and commonly applied models, the

pseudo-first-order and pseudo-second-order [44, 45]. The mathematical expression of these models, their respective supporting parameters and the import of the respective model parameters (at different initial adsorbate concentrations) to the present adsorption system are discussed elaborately in the following subsections. The judgement on the goodness of fit of the respective model is made based on the magnitude of the APE- values which are evaluated from Eq. (5).

Pseudo-first-order (PFO) model

The PFO [46] postulates that the adsorption rate constant (k_1) varies inversely as the adsorbate concentration (c_e), with a characteristic first-order reaction mechanism. The nonlinear form of the PFO model is presented in Eq. (12).

$$q_t = q_e [1 - \exp(-k_1 t)] \quad (12)$$

The models' plot and the corresponding parameters obtained for the 400 and 500 mg/L adsorption system are presented in Fig. 6; Table 3, respectively. Observation from the Table showed that the rate constant (k_1) and calculated adsorption capacity ($q_{e, cal}$) increased correspondingly as the initial concentration. Meanwhile, theoretical maximum adsorption capacity ($q_{e, Cal}$) values of 370.34 mg/g (for 400 mg/L system) and 420.0 mg/g (for 500 mg/L system) are consistent with the experimentally derived uptake amount ($q_{e @ 400 \text{ mg/L}} = 368.76$ mg/g and $q_{e @ 500 \text{ mg/L}} = 419.79$ mg/g). Furthermore, the coefficient of determination (R^2) was in all cases greater than 0.9, while relatively low APE values were also recorded. These results are indications of the good fitting of the PFO model. The experiment-isotherm plot shown in Fig. 6 depicted a close correlation between the experimental curve and the PFO model curve, an indication for the PFO model prediction adequacy.

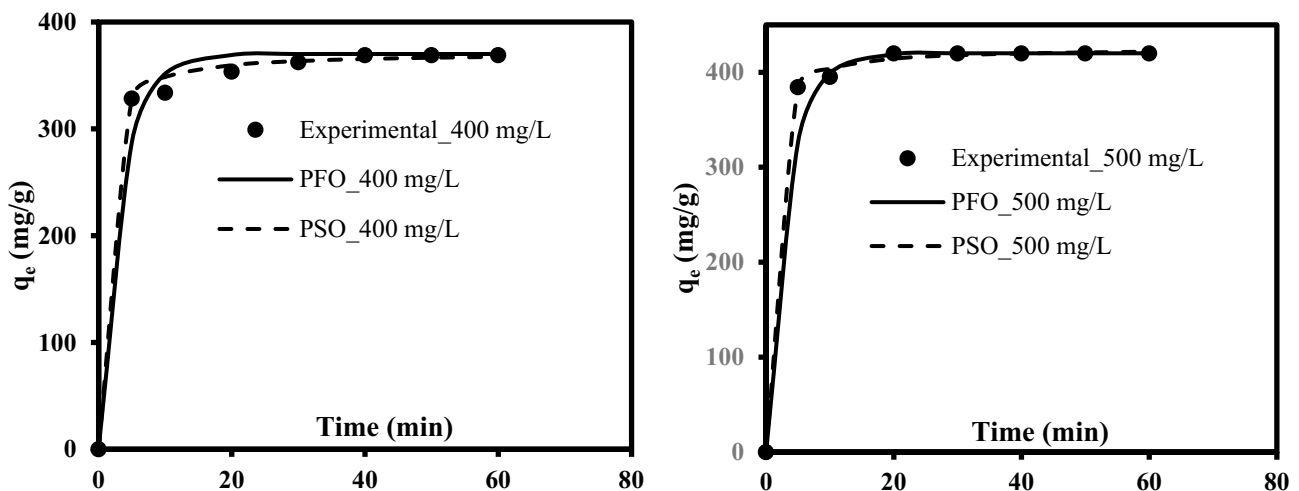


Fig. 6 Plots of the Experimental, Pseudo-first-order, and Pseudo-second-order kinetics data at varying initial concentrations

Table 3 Kinetic model parameters

Pseudo-first order	Pseudo-second order
400 mg/L	
$q_e = 370.34$	$q_e = 371.33$
$k_1 = 0.300$	$k_2 = 0.004$
$R^2 = 0.997$	$R^2 = 0.999$
$APE = 0.253$	$APE = 0.082$
500 mg/L	
$q_e = 420.00$	$q_e = 425.43$
$k_1 = 0.310$	$k_2 = 0.004$
$R^2 = 0.997$	$R^2 = 0.999$
$APE = 0.164$	$APE = 0.046$

NB: $q_{e, \text{exp}} = 368.76$ mg/g (for 400 mg/L system) and 419.79 mg/g (for 500 mg/L system)

Pseudo-second-order (PSO) model

The PSO [47] model assumes that the adsorption rate is a direct function of the available adsorption sites on the adsorbent and also provides information on the adsorbents' adsorption capacity. The PSO nonlinear equation is expressed as Eq. (13).

$$q_t = \frac{k_2 * q_e^2 * t}{(1 + k_2 * t)} \quad (13)$$

The models' plot and the corresponding parameters obtained for the 400 and 500 mg/L adsorption system are presented in Fig. 6; Table 3, respectively. In comparison with the PFO data, the PSO model depicted lower APE values and higher R^2 -values; thus, it provides a better fit to the experimental data. Just like in the case of the PFO model, its adsorption capacity increased as the initial adsorbate concentration, however, the k_2 -value remained constant for both adsorption systems (Table 3). This signifies that the PSO rate constant (k_2) is independent of bulk liquid phase metal ion concentration, with increased adsorbate-adsorbent affinity as the initial concentration increased. The experiment-isotherm plot shown in Fig. 6 depicted a closer correlation between the experimental curve and the PSO model curve when compared with that of the PFO model. Therefore, it is believed that the PSO model provided the best fit to the experimental kinetic data.

Conclusions

Hydrogel based adsorbent ('Poly-g-Hyd') was successfully synthesized via the saponification of acrylonitrile grafted starch precursor. The extent of the initial copolymer grafting was determined from the % nitrogen content of the graft

product. Meanwhile, due to the transformation of some of the cyano groups on the grafted starch to amide (-CONH₂) and carboxylate (-COONa) groups, the synthesized hydrogel ('Poly-g-Hyd') depicted a lower % nitrogen content when compared to that of the grafted starch. Furthermore, the 'Poly-g-Hyd' showed a relatively high-water absorption capacity of 490 g water/g 'Poly-g-Hyd', which could be due to the structural changes occurring during the sequential stages of gelatination and crosslinking involved in the adsorbent synthesis protocol. The maximum zinc ion uptake was recorded at pH 5.0, 20 min and 0.3 g/L adsorbent concentrations. The adsorption experimental data was effectively modelled using equilibrium and kinetic models, while the effect of some process variables on the 'Poly-g-Hyd' adsorption capacity was also elucidated in the study.

Data availability statement The raw/processed data required to reproduce these findings cannot be shared at this time as the data also forms part of an ongoing study.

References

1. Hashem A, Aniagor CO, Badawy SM, Taha GM (2021) Novel application of the esterification product of 2, 3-dihydroxybutanedioic acid and cellulosic biomass for cobalt ion adsorption. *Korean J Chem Eng.* <https://doi.org/10.1007/s11814-021-0872-7>
2. Hashem A, Al-Anwar A, Nagy NM, Hussein DM, Eisa S (2016) Isotherms and kinetic studies on adsorption of Hg (II) ions onto *Ziziphus spina-christi* L. from aqueous solutions. *Green Process Synth* 5(2):213–224
3. Hashem A, Badawy SM, Farag S, Mohamed LA, Fletcher AJ, Taha GM (2020) Non-linear adsorption characteristics of modified pine wood sawdust optimised for adsorption of Cd (II) from aqueous systems. *J Environ Chem Eng* p. 103966
4. Deliyanni E, Peleka E, Matis K (2007) Removal of zinc ion from water by sorption onto iron-based nanoadsorbent. *J Hazard Mater* 141(1):176–184
5. Abdel-Halim E, Al-Deyab SS (2014) Preparation of poly (acrylic acid)/starch hydrogel and its application for cadmium ion removal from aqueous solutions. *React Funct Polym* 75:1–8
6. Jain C (1996) Application of chemical mass balance to upstream/downstream river monitoring data. *J Hydrol* 182(1–4):105–115
7. Hashem A, Abdel-Lateff A, Farag S, Hussein D (2008) Treatment of alhagi residues with tartaric acid for the removal of Zn (II) ions from aqueous solution. *Adsorp Sci Technol* 26(9):661–678
8. Chakraborty R, Asthana A, Singh AK, Jain B, Susan AB (2020) Adsorption of heavy metal ions by various low-cost adsorbents: a review. *Int J Environ Anal Chem* p. 1–38
9. Srivastava VC, Mall ID, Mishra IM (2008) Removal of cadmium (II) and zinc (II) metal ions from binary aqueous solution by rice husk ash. *Colloids Surf A Physicochem Eng Asp* 312(2–3):172–184
10. Hawari A, Rawajfih Z, Nsour N (2009) Equilibrium and thermodynamic analysis of zinc ions adsorption by olive oil mill solid residues. *J Hazard Mater* 168(2–3):1284–1289
11. Aniagor CO, Elshkankery M, Fletcher A, Morsy OM, Abdel-Halim E, Hashem A (2021) Equilibrium and Kinetic Modelling of

- Aqueous Cadmium Ion and Activated Carbon Adsorption System. *Water Conserv Sci Eng* 6:95–104
12. Mohamed LA, Aniagor CO, Hashem A (2021) Isotherms and kinetic modelling of mycoremediation of hexavalent chromium contaminated wastewater. *Cleaner Engineering Technology* 4:100192
 13. Wang J, Chen C (2009) Biosorbents for heavy metals removal and their future. *Biotechnol Adv* 27(2):195–226
 14. Božić D, Gorgievski M, Stanković V, Štrbac N, Štrbula S, Petrović N (2013) Adsorption of heavy metal ions by beech sawdust—Kinetics, mechanism and equilibrium of the process. *Ecol Eng* 58:202–206
 15. Mohammed RR (2012) Removal of heavy metals from waste water using black tea waste. *Arab J Sci Eng* 37(6):1505–1520
 16. Hashem A, Aniagor C, Taha G, Fikry M, Utilization of Low-cost Sugarcane Waste for the Adsorption of Aqueous Pb(II): Kinetics and Isotherm Studies. *Current Research in Green Sustainable Chemistry*, 2021. 4, 100056, <https://doi.org/10.1016/j.crgsc.2021.100056>
 17. Hashem A, Fletcher A, El-Sakhawy M, Mohamed LA, Farag S (2020) Aminated Hydroxymoyl Camelthorn Residues as a Novel Adsorbent for Extracting Hg (II) From Contaminated Water: Studies of Isotherm, Kinetics, and Mechanism. *J Polym Environ* 28(9):2498–2510
 18. Wang J, Zhuang S (2017) Removal of various pollutants from water and wastewater by modified chitosan adsorbents. *Crit Rev Environ Sci Technol* 47(23):2331–2386
 19. Aniagor CO, Afifi M, Hashem A (2021) Rapid and efficient uptake of aqueous lead pollutant using starch-based superabsorbent hydrogel. *Polym Bull.* <https://doi.org/10.1007/s00289-021-03817-4>
 20. Hashem A, Aniagor C, Hussein D, Farag S (2021) Application of novel butane-1, 4-dioic acid-functionalized cellulosic biosorbent for aqueous cobalt ion sequestration. *Cellulose* 28:3599–3615
 21. Hashem A, Aniagor CO, Afifi MAF, Abou-Okeil A, Samaha SH (2021) Synthesis of super-absorbent poly (AN)-g-starch composite hydrogel and its modelling for aqueous sorption of cadmium ions. *Korean J Chem Eng.* <https://doi.org/10.1007/s11814-021-0856-7>
 22. Zhou Y, Fu S, Zhang L, Zhan H, Levit MV (2014) Use of carboxylated cellulose nanofibrils-filled magnetic chitosan hydrogel beads as adsorbents for Pb (II). *Carbohydr Polym* 101:75–82
 23. Abdel-Halim ES (2013) Preparation of starch/poly(N,N-Diethylaminoethyl methacrylate) hydrogel and its use in dye removal from aqueous solutions. *React Funct Polym* 73(11):1531–1536
 24. Kjeldahl JG (1883) Neue methode zur bestimmung des stickstoffs in organischen körpern. *Zeitschrift für analytische Chemie* 22(1):366–382
 25. Hashem A, Afifi M, El-Alfy E, Hebeish A (2005) Synthesis, characterization and saponification of poly (AN)-starch composites and properties of their hydrogels. *Am J Appl Sci* 2(3):614–621
 26. Asuquo E, Martin A, Nzerem P, Siperstein F, Fan X (2017) Adsorption of Cd (II) and Pb (II) ions from aqueous solutions using mesoporous activated carbon adsorbent: Equilibrium, kinetics and characterisation studies. *J Environ Chem Eng* 5(1):679–698
 27. Aniagor C, Abdel-Halim E, Hashem A (2021) Evaluation of the aqueous Fe (II) ion sorption capacity of functionalized microcrystalline cellulose. *J Environ Chem Eng* 9(4):105703
 28. Igwegbe CA, Oba SN, Aniagor CO, Adeniyi AG, Ighalo JO (2020) Adsorption of ciprofloxacin from water: a comprehensive review. *J Ind Eng Chem* 93:57–77
 29. Kuang Y, Zhang X, Zhou S (2020) Adsorption of methylene blue in water onto activated carbon by surfactant modification. *Water* 12(2):587
 30. Aniagor CO, Sokker H, Hashem A, El-Hamaki Y, El-Degwi M, Abdel-Halim E, Hashem A (2021) Equilibrium studies on the uptake of nitrate and phosphate ions using functionalized carbon cloth. *J Radioanal Nucl Chem* 329:1091–1102
 31. Girish C, Murty VR (2016) Mass transfer studies on adsorption of phenol from wastewater using *Lantana camara*, forest waste. *Int J Chem Eng.* <https://doi.org/10.1155/2016/5809505> (Article ID 5809505)
 32. Pekař M (2020) Thermodynamic driving forces and chemical reaction fluxes; reflections on the steady state. *Molecules* 25(3):699
 33. Prah A, Frančišković E, Mavri J, Stare J (2019) Electrostatics as the driving force behind the catalytic function of the monoamine oxidase a enzyme confirmed by quantum computations. *ACS Catal* 9(2):1231–1240
 34. Wang J, Guo X (2020) Adsorption isotherm models: Classification, physical meaning, application and solving method. *Chemosphere* p. 127279
 35. Langmuir I (1916) The constitution and fundamental properties of solids and liquids. Part I. Solids. *J Am Chem Soc* 38(11):2221–2295
 36. Adamson AW, Gast AP (1967) *Physical chemistry of surfaces*, vol 150. Interscience publishers New York
 37. Temkin M (1940) Kinetics of ammonia synthesis on promoted iron catalysts. *Acta Physiochim URSS* 12:327–356
 38. Radushkevich M (1947) The equation of the characteristic curve of the activated charcoal USSR. *Phys Chem Sec* 55:331
 39. Günay A, Arslankaya E, Tosun I (2007) Lead removal from aqueous solution by natural and pretreated clinoptilolite: adsorption equilibrium and kinetics. *J Hazard Mater* 146(1–2):362–371
 40. Dąbrowski A (2001) Adsorption—from theory to practice. *Adv Colloid Interface Sci* 93(1–3):135–224
 41. Dubinin M (1960) The potential theory of adsorption of gases and vapors for adsorbents with energetically nonuniform surfaces. *Chem Rev* 60(2):235–241
 42. Wang G, Chang Q, Zhang M, Han X (2013) Effect of pH on the removal of Cr (III) and Cr (VI) from aqueous solution by modified polyethyleneimine. *React Funct Polym* 73(11):1439–1446
 43. Jiang M, Yang W, Zhang Z, Yang Z, Wang Y (2015) Adsorption of three pharmaceuticals on two magnetic ion-exchange resins. *J Environ Sci* 31:226–234
 44. Wang J, Guo X (2020) Adsorption kinetic models: Physical meanings, applications, and solving methods. *J Hazard Mater* 390:122156
 45. Guo X, Wang J (2019) A general kinetic model for adsorption: theoretical analysis and modeling. *J Mol Liq* 288:111100
 46. Aniagor CO, Afifi MA, Hashem A (2021) Modelling of basic blue-9 dye sorption onto hydrolyzed polyacrylonitrile grafted starch composite. *Carbohydrate Polymer Technologies Applications* 2:100141. <https://doi.org/10.1016/j.carpta.2021.100141>
 47. Ho Y-S, McKay G (1999) Pseudo-second order model for sorption processes. *Process Biochem* 34(5):451–465

Publisher's Note Springer Nature remains neutral with regard to jurisdictional claims in published maps and institutional affiliations.